Comparison of Electrically Excited Synchronous Machines Using Copper and Aluminum Windings in Stator and Rotor

Tianzheng Xiao, *Member*, *IEEE*, Zi Qiang Zhu, *Fellow*, *IEEE*, and Ziad Azar

***Abstract*—In this paper, electrically excited synchronous machines (EESMs) using copper (Cu) and aluminum (Al) windings are compared for the feasibility of replacing Cu windings with Al windings in electric vehicle (EV) applications since Al windings have lower mass density and cost per weight, but higher resistivity and lower thermal conductivity than Cu windings. The EESMs with four winding configurations are optimized with an electromagnetic-thermal co-optimization method. The optimized EESM with only Cu windings is considered as the baseline in this study. Results show that the EESM with stator-Cu/rotor-Al windings has the least torque reduction (12.1%) compared to the baseline among the three EESMs with Al windings and the highest torque mass density among all EESMs. Meanwhile, although the new European driving cycle efficiency of the stator-Cu/rotor-Al EESM is 1.8% lower than that of the baseline, the torque per cost is 71% higher, and the maximum rotor mechanical stress is 8% lower. Therefore, the EESMs with stator-Cu/rotor-Al windings are prospective substitutions of those with only Cu windings for EV applications considering the trade-off between performance and cost..**

***Index Terms*—Aluminum winding, Copper winding, Cost efficiency, Electrically excited synchronous machines, Torque density, Winding temperature.**

NOMENCLATURE

A_{wp}	Area of winding cross section
B_m	Flux density amplitude in p_{iron}
B_{wp}, C_{wp}, X_{wp}, Y_{wp}	Functions related to geometry and thermal properties
f	Frequency in p_{iron}
g	Airgap length
h_{air}	Heat transfer coefficient between iron cores and airgap
H_{wp}	Height of rectangular winding cross section
i	Number of an arbitrary operation point in driving cycle
$I_{a/f}$	Armature/field winding currents
$k_{h/e/exc}$	Coefficients of hysteresis/eddy current/excessive losses in p_{iron}
K_n, D_n, E_n, F_n	Coefficients in $\vartheta_{wp}(r, \theta)$
L_{stk}	Stack length
n, k	Order numbers in K_n, D_n, E_n, and F_n, as well as in the Fourier forms of B_{wp}, C_{wp}, X_{wp}, and Y_{wp}
N	Total number of operation points in driving cycle efficiency calculation
N_p, N_s	Pole and slot numbers
Nu, *Ta*, *Re*, *Pr*	Nusselt's, Taylor's, Reynold's, and Prandtl's numbers
p_{iron}	Iron loss mass density
$P_{iron\_s/r}$	Iron losses of stator/rotor cores
P_{Out_i}, P_{Loss_i}	Output power and loss of the i^{th} point in driving cycle efficiency calculation
P_{Re}	Resistive loss
$P_{Re\_s/r}$	Resistive losses of stator/rotor
$P_{Re\_saw/sew/raw/rew}$	Resistive losses of stator active/stator end/rotor active/rotor end windings
P_{wp}	Resistive loss of winding part
$R_{a/f}$	Armature/field winding resistances
$R_{fr\_c/sc/a/sh}$	Thermal resistances between frame and coolant/stator core/ambient/shaft
$R_{raw\_ag/ew}$	Thermal resistances between rotor active winding and airgap/rotor end winding
$R_{rc\_raw/ag}$	Thermal resistances between rotor core and rotor active winding/airgap
$R_{saw\_ag/ew}$	Thermal resistances between stator active winding and airgap/stator end winding
$R_{sc\_saw/ag}$	Thermal resistances between stator core and stator active winding/airgap
R_{sew/rew_c}	Thermal resistances between stator/rotor end windings and coolant
R_{sh_rc}	Thermal resistances between shaft and rotor core
$R_{so/si/ro/ri}$	Stator outer/stator inner/rotor outer/rotor inner radii
r_{wp_max}	Radial position where maximum temperature appears
$R_{wp\_o/i}$	Outer/inner radii of sector winding cross section
t_{ps}	Pole shoe thickness
t_{ry}	Rotor yoke thickness
t_{sy}	Stator yoke thickness
$V_{saw/sew/raw/rew}$	Volumes of stator active/stator end/rotor active/rotor end windings
V_{wp}	Volume of winding part
w_p	Rotor pole width
w_t	Stator tooth width
W_{wp}	Width of rectangular winding cross section
α	Pole arc ratio of rotor pole shoe
β_I	Current phase angle
γ	Ratio of P_{Re_s} to P_{Re_r}
η_{NEDC}	Driving cycle efficiency under New European Driving Cycle
$\vartheta_{a/frc/ewc}$	Ambient/frame water cooling/end winding spray oil temperatures
$\vartheta_{max/avg\_sec/rec}$	Maximum/average temperature of sector/rectangular winding cross sections
ϑ_{max_all}	The highest one among the maximum temperatures of stator active winding, rotor active winding, stator end winding, and rotor end winding

Manuscript received January 5, 2026; revised February 9, 2026; accepted March 2, 2026. Date of publication March 25, 2026; Date of current version March 23, 2026.

This work was supported in part by China Scholarship Council (CSC) under Grant 202206160023.

Tianzheng Xiao is with the School of Electrical and Electronic Engineering, the University of Sheffield, Sheffield, S1 3JD, UK (e-mail: txiao5@sheffield.ac.uk).

Zi Qiang Zhu is with the Department of Electrical and Electronic Engineering, the Hongkong Polytechnic University, 11 Yuk Choi Rd, Hung Hom, Hong Kong, China (e-mail: z.q.zhu@polyu.edu.hk).

Ziad Azar is with Siemens Energy Industrial Turbomachinery Ltd., Ruston House, Waterside South, Lincoln, LN5 7FD, UK (e-mail: ziad.azar@siemens-energy.com).

(*Corresponding Author: Zi Qiang Zhu*)

Digital Object Identifier 10.30941/CESTEMS.2026.00008

$\vartheta_{max\_saw/sew/raw/rew}$	Maximum temperatures of stator active/stator end/rotor active/rotor end windings
$\vartheta_{saw/sew/raw/rew}$	Average temperatures of stator active/stator end/rotor active/rotor end windings
$\vartheta_{sc/rc/ag/fr}$	Average temperatures of stator core/rotor core/airgap/frame
$\vartheta_{sw/rw}$	Temperatures of stator winding/rotor winding
θ_{wp}	Angle of sector winding cross section
$\vartheta_{wp}(r, \theta)$	Temperature distribution of sector winding cross section in r-θ coordinate
$\vartheta_{wp\_I/II/III/IV}$	Temperature boundary conditions of winding cross section
λ_{air}, ν_{air}, α_{air}	Thermal conductivity, kinematic viscosity, and thermal diffusivity of air
λ_{wp_c}	Thermal conductivity on cross section
$\rho_{Cu/Al}$	Resistivities of copper/aluminum windings
σ	Split ratio
ω_m	Rotor angular speed

I. Introduction

As the supply of rare-earth magnets is instable in global market, electrically excited synchronous machines (EESMs) are gaining more attention as a substitution of permanent magnet synchronous machines (PMSMs) in applications such as passenger electric vehicles (EVs) [1]-[2], heavy-duty trucks [3]-[4], and aircraft starter-generators [5]-[6] due to advantages of zero rare-earth usage, lower cost, excellent overload capability, good rotor flux regulation ability, nearly unity power factor, and feasible constant power operation [7]-[8].

In recent years, the feasibility of aluminum (Al) windings has been investigated in [9]-[10] for EESMs and in [11]-[13] for other types of electrical machines due to lower mass density, lower price per weight, better flexibility in manufacture, and better sustainability than copper (Cu) windings, while Al also has higher electric resistivity, lower thermal conductivity, and provides a trade-off between direct current (DC) and alternating current (AC) copper losses [14]-[15]. In [9], the EESMs with only Cu windings and with only Al windings on stator and rotor are designed and compared to replace an interior permanent magnet (IPM) benchmark for a heavy-duty truck application. Although the Al winding EESM shows similar performance, higher power density, and lower winding cost compared to the Cu winding EESM, the winding temperatures of all EESMs are not studied, which is a major difference between Al and Cu windings. In [10], four EESMs with Cu/Al windings on stators and/or rotors are compared for EV application. However, for convenience, the EESMs with Al windings share the same iron cores as that with only Cu windings, which may not be optimal designs. Although winding temperatures are analyzed and compared in [10], the torque density and cost efficiency of all EESMs are not compared, which are the benefits of Al windings. In [9]-[10], rotor mechanical stress is not studied, while Al windings have such a benefit when installed in the rotor due to lower mass density.

To thoroughly investigate the differences in performance, weight, cost, and rotor mechanical stress among the EESMs with Cu/Al windings in stator and/or rotor for EV applications, the EESMs are designed using a coupled electromagnetic-thermal co-optimization method based on a commercial IPM benchmark [16]. The total resistive loss and cooling conditions of all EESMs are the same. The input currents are determined based on calculated winding temperatures and resistances. The electromagnetic performances, driving cycle efficiencies, weights, costs, and rotor mechanical stresses of all EESMs are then compared. The differences and similarities of this paper and previous papers [9]-[10] are summarized in Table I.

TABLE I
SUMMARY OF EXISTING PAPERS ON EESMS WITH CU AND/OR AL WINDINGS

Item/comparison	[8]	[9]	This paper
Stator/rotor winding	Cu-only & Al-only	Cu/Al on stator and/or rotor	
Design optimization	Torque-weight-cost	×	Torque-thermal
Torque & efficiency	√	√	√
Torque density	√ (power density)	×	√
Cost efficiency	Cost only	×	√
Temperature	×	√	√
Rotor core stress	×	×	√
Conclusion	Al-only EESM has similar efficiency, higher power density, and less winding cost than Cu-only EESM	EESMs with Al windings have close efficiency to the Cu-only one, but need better cooling measures	Stator-Cu/rotor-Al EESM can replace the Cu-only one with higher torque density and cost efficiency, and less rotor core stress

This paper is structured as follows. The coupled electromagnetic-thermal co-optimization method is introduced in Section II. The co-optimizations of all EESMs are conducted in Section III. All optimized EESMs are compared in Section IV. The conclusions and future work are given in Section V.

II. Coupled Electromagnetic-thermal Co-optimization of EESMs

In this section, the coupled electromagnetic-thermal co-optimization method for the design of EESMs is introduced. The procedure of co-optimization method is presented in Fig. 1. The electromagnetic part is the two-dimensional (2-D) finite element analysis (FEA) and the genetic algorithm (GA) for design optimization in ANSYS Electronics Desktop 2021 R2. The thermal part consists of a steady-state lumped parameter thermal network (LPTN) and analytical formulae for winding maximum temperature based on average temperature.

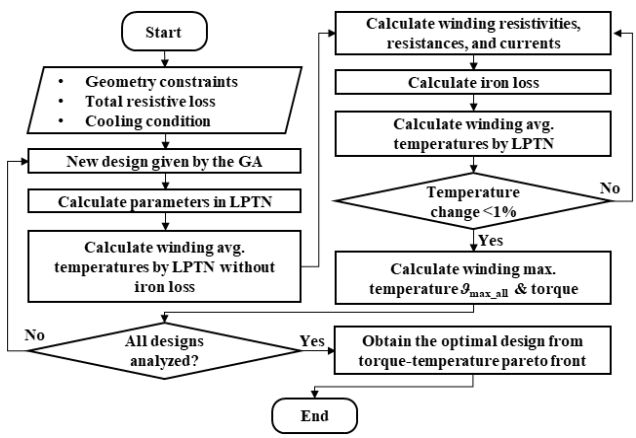

Fig. 1. Procedure diagram of coupled electromagnetic-thermal co-optimization method for EESMs.

In the co-optimization of EESMs, the steady-state LPTN is firstly solved without iron loss. Then, winding resistances and currents are calculated, and iron losses are evaluated using the classic 3-term iron loss (1) [17], after which the LPTN is solved repeatedly with iron losses until the temperature variation is less than 1%. p_{iron}, B_{m}, k_{h}, k_{e}, k_{exc}, and f in (1) are the iron loss mass density, the flux density, the hysteresis loss coefficient, the eddy current loss coefficient, the excessive loss coefficient, and the frequency, respectively. The maximum-average winding temperature formulae are then used to calculate the maximum temperatures of all winding parts. The highest one among the maximum temperatures of stator active winding, rotor active winding, stator end winding, and rotor end winding ($\vartheta_{\text{max\_all}}$) will be output with torque. After all designs are analyzed, the optimal design is obtained on the temperature-torque pareto front. The heat transfer of EESMs and the corresponding LPTN in this study are shown in Fig. 2 with all abbreviations noted. The cooling strategies include frame water jacket cooling and end winding spray oil cooling, which are common for EV traction motors [18].

$$p_{\text{iron}} = k_{\text{h}} f B_{\text{m}}^2 + k_{\text{e}} f^2 B_{\text{m}}^2 + k_{\text{exc}} f^{1.5} B_{\text{m}}^{1.5} \tag{1}$$

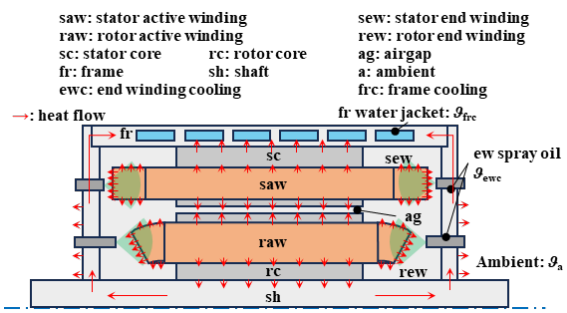

(a)

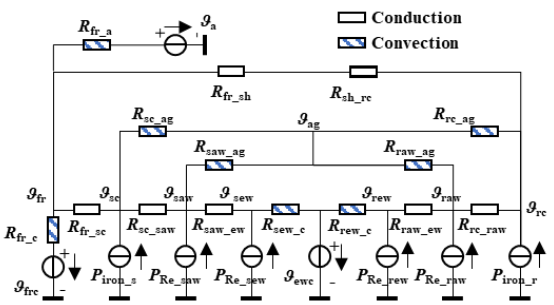

(b)

Fig. 2. Heat transfer of EESMs for EV application. (a) Heat transfer diagram of EESMs. (b) Corresponding steady-state LPTN.

While the LPTN is unable to predict the winding maximum temperatures without refinement for windings, the analytical formulae for winding maximum temperatures based on average temperatures are derived in [19]. As presented in Fig. 3, the sector cross section is for stator active windings, rotor active windings, and rotor end windings, while the rectangular cross section is for the end part of overlapping windings. $R_{\text{wp\_o/i}}$, θ_{wp}, H_{wp}, W_{wp}, $\vartheta_{\text{wp\_I/II/III/IV}}$, P_{wp}, and V_{wp} are the outer/inner radii of sector, the angle of sector, the height of rectangular, the width of rectangular, the temperature boundary conditions (TBCs), the resistive loss of winding part, and the volume of winding part, respectively. It is proved in [19] that the influence of TBCs can be ignored when P_{wp} dominates the winding temperature rise, so the calculation of maximum temperature $\vartheta_{\text{max\_sec}}/\vartheta_{\text{max\_rec}}$ based on average temperature $\vartheta_{\text{avg\_sec}}/\vartheta_{\text{avg\_rec}}$ is given by (2)/(3) for sector/rectangular cross section case. The functions B_{wp}, C_{wp}, X_{wp}, and Y_{wp} related to geometry and thermal properties in (2) and (3) are given by (4)-(12). $\vartheta_{\text{wp}}(r, \theta)$, $r_{\text{wp\_max}}$, A_{wp}, and $\lambda_{\text{wp\_c}}$ are the temperature distribution of sector cross section, the radial position where maximum temperature appears, the area of winding part cross section, and the thermal conductivity on cross section, respectively. K_n, D_n, E_n, and F_n in (8)-(10) are the coefficients in the temperature distribution $\vartheta_{\text{wp}}(r, \theta)$.

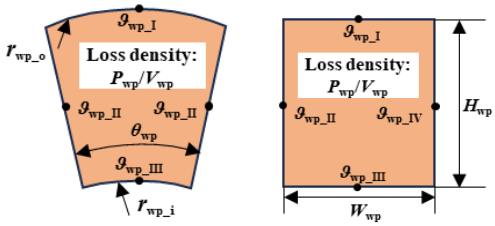

(a) (b)

Fig. 3. Winding cross sections. (a) Sector cross section in r-θ coordinate. (b) Rectangular cross section in x-y coordinate.

$$\vartheta_{\text{max\_sec}} - \vartheta_{\text{avg\_sec}} = \frac{P_{\text{wp}}}{V_{\text{wp}}}\left(B_{\text{wp}} - C_{\text{wp}}\right) \tag{2}$$

$$\vartheta_{\text{max\_rec}} - \vartheta_{\text{avg\_rec}} = \frac{P_{\text{wp}}}{V_{\text{wp}}}\left(X_{\text{wp}} - Y_{\text{wp}}\right) \tag{3}$$

$$B_{\text{wp}} = \sum_{n=1} D_n r_{\text{wp\_max}}^{K_n} + E_n r_{\text{wp\_max}}^{-K_n} + \frac{P_{\text{wp}} F_{\text{n}}}{V_{\text{wp}} \lambda_{\text{wp\_c}}} r_{\text{wp\_max}}^2 \tag{4}$$

$$C_{\text{wp}} = \iint_{r_{\text{wp\_i}}, -0.5\theta_{\text{wp}}}^{r_{\text{wp\_o}}, 0.5\theta_{\text{wp}}} \frac{2\vartheta_{\text{wp}}(r,\theta)}{0.5\theta_{\text{wp}}\left(r_{\text{wp\_o}}^2 - r_{\text{wp\_i}}^2\right) A_{\text{wp}}} r \mathrm{d}r \mathrm{d}\theta \tag{5}$$

$$r_{\text{wp\_max}} \approx 0.5\left(r_{\text{wp\_o}} + r_{\text{wp\_i}}\right) \tag{6}$$

$$\vartheta_{\text{wp}}(r,\theta) = \vartheta_{\text{wp\_II}} + \sum_{n=1}\left(D_n r^{K_n} + E_n r^{-K_n} + \frac{P_{\text{wp}} F_n r^2}{V_{\text{wp}} \lambda_{\text{wp\_c}}}\right)\cos\left(K_n\theta\right) \tag{7}$$

$$K_n = \frac{(2n-1)\pi}{0.5\theta_{\text{wp}}} \tag{8}$$

$$\begin{bmatrix} D_n \\ E_n \end{bmatrix} = \begin{bmatrix} r_{\text{wp\_o}}^{K_n} & r_{\text{wp\_o}}^{-K_n} \\ r_{\text{wp\_i}}^{K_n} & r_{\text{wp\_i}}^{-K_n} \end{bmatrix}^{-1} \begin{bmatrix} \dfrac{\int\left(\vartheta_{\text{wp\_I}} - \vartheta_{\text{wp\_II}}\right)\cos\left(K_n\theta\right)\mathrm{d}\theta}{\int\cos^2\left(K_n\theta\right)d\theta} - \dfrac{P_{\text{wp}} F_n r_{\text{wp\_o}}^2}{V_{\text{wp}}\lambda_{\text{wp\_c}}} \\ \dfrac{\int\left(\vartheta_{\text{wp\_III}} - \vartheta_{\text{wp\_II}}\right)\cos\left(K_n\theta\right)\mathrm{d}\theta}{\int\cos^2\left(K_n\theta\right)\mathrm{d}\theta} - \dfrac{P_{\text{wp}} F_n r_{\text{wp\_i}}^2}{V_{\text{wp}}\lambda_{\text{wp\_c}}} \end{bmatrix} \tag{9}$$

$$F_n = \frac{\theta_{\text{wp}} \sin\left(0.25\theta_{\text{wp}} K_n\right)}{K_n\left(K_n^2 - 4\right)} \tag{10}$$

$$X_{\text{wp}} = \sum_{n,k=1} \frac{16\sin\left(\dfrac{n\pi H_{\text{wp}}}{2W_{\text{wp}}}\right)\sin\left(\dfrac{k\pi W_{\text{wp}}}{2H_{\text{wp}}}\right)}{nk\pi^2\lambda_{\text{wp\_c}}\left[\left(\dfrac{n\pi}{W_{\text{wp}}}\right)^2 + \left(\dfrac{k\pi}{H_{\text{wp}}}\right)^2\right]} \tag{11}$$

$$Y_{\mathrm{wp}}=\sum_{n,k=1}\frac{64}{n^2k^2\pi^4\lambda_{\mathrm{wp\_c}}\left[\left(\frac{n\pi}{W_{\mathrm{wp}}}\right)^2+\left(\frac{k\pi}{H_{\mathrm{wp}}}\right)^2\right]} \tag{12}$$

III. Co-optimization of EESMs

In this section, the EESMs with Cu/Al windings in stator and/or rotor are designed using the co-optimization method introduced in Section II.

A. Design Specifications of EESMs

The cross section of EESMs is presented in Fig. 4 with all the geometrical parameters marked. Apart from those parameters, the stack length L_{stk}, the current phase angle β_{I}, and the ratio γ of stator resistive loss $P_{\mathrm{Re\_s}}$ to rotor resistive loss $P_{\mathrm{Re\_r}}$ are also optimized. N_{p} in Fig. 4 is the pole number.

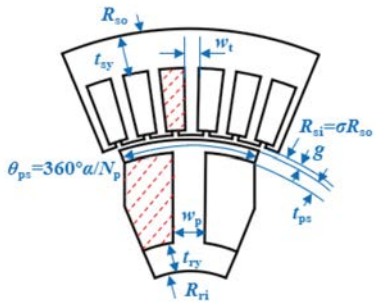

Fig. 4. Cross section and geometry parameters of EESMs.

In the design optimization of the EESMs, the stator outer radius R_{so}, the rotor inner radius R_{ri}, the airgap length g, slot/pole numbers L_{stk}, and the total resistive loss P_{Re} are fixed to the same as the IPM benchmark in [16], which is shown in Fig. 5. The values and ranges of all parameters are listed in Table II. The H-class insulation is adopted, which fails at higher than 180 °C.

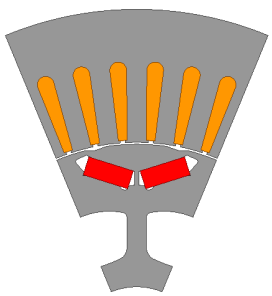

Fig. 5. Cross section of IPM benchmark.

The resistivities of Cu and Al windings ρ_{Cu} and ρ_{Al} are calculated by (13), where $\vartheta_{\mathrm{sw/rw}}$ is the volume weighted average of stator/rotor active winding and end winding average temperatures calculated by (14). The armature and field excitation currents I_{a} and I_{f} are then calculated by (15).

$$\begin{cases}\rho_{\mathrm{Cu}}=1.70\times\left[1+0.0039\left(\vartheta_{\mathrm{sw/rw}}-20\right)\right]\ (10^{-8}\Omega\cdot\mathrm{m}^{-1})\\ \rho_{\mathrm{Al}}=2.82\times\left[1+0.0043\left(\vartheta_{\mathrm{sw/rw}}-20\right)\right]\ (10^{-8}\Omega\cdot\mathrm{m}^{-1})\end{cases} \tag{13}$$

$$\vartheta_{\mathrm{sw/rw}}=\frac{V_{\mathrm{saw/raw}}\vartheta_{\mathrm{saw/raw}}+V_{\mathrm{sew/rew}}\vartheta_{\mathrm{sew/rew}}}{V_{\mathrm{saw/raw}}+V_{\mathrm{sew/rew}}} \tag{14}$$

TABLE II
VALUES/RANGES OF ALL PARAMETERS IN DESIGN CO-OPTIMIZATION OF EESMS

Parameter	Value/range
Stator outer radius, R_{so}/mm	132
Rotor inner radius, R_{ri}/mm	45
Stack length, L_{stk}/mm	50.2
Airgap length, g/mm	0.73
Pole shoe thickness, t_{ps}/mm	8
Slot/pole numbers, $N_{\mathrm{s}}/N_{\mathrm{p}}$	48/8
Stator winding turn number per phase	88
Stator slot filling factor	0.40
Rotor winding total turn number	88
Rotor slot filling factor	0.55
Total resistive loss, P_{Re}/W	8455
Rotor speed/(r/min)	3750
Winding insulation class	H (180 °C)
Stator yoke thickness, t_{sy}/mm	10 to 25
Stator tooth width, w_{t}/mm	5 to 11
Stator current phase angle, β_{I}/(°)	−30 to 30
Ratio γ of $P_{\mathrm{Re\_s}}$ to $P_{\mathrm{Re\_r}}$	0.25 to 4
Split ratio, σ	0.6 to 0.9
Pole arc ratio of pole shoe, α	0.5 to 1
Rotor pole width, w_{p}/mm	15 to 40.5
Rotor yoke thickness, t_{ry}/mm	10 to 30
Winding temperatures	Calculated by LPTN
Winding resistivities	Calculated by (12)
Winding resistances, R_{a} and R_{f}	Geometry and resistivities
Winding currents, I_{a} and I_{f}	Calculated by (14)

$$\begin{cases}I_{\mathrm{a}}=P_{\mathrm{Re\_s}}/3R_{\mathrm{a}}\\ I_{\mathrm{f}}=P_{\mathrm{Re\_r}}/R_{\mathrm{f}}\end{cases} \tag{15}$$

where $V_{\mathrm{saw/raw/sew/rew}}$ is the volume of stator active windings/rotor active windings/stator end windings/rotor end windings. $\vartheta_{\mathrm{saw/raw/sew/rew}}$ is the average temperature of stator active windings/rotor active windings/stator end windings/rotor end windings calculated by LPTN. $R_{\mathrm{a/f}}$ is the resistance of armature windings/field windings.

The cooling conditions are listed in Table III based on the typical values of flow rates and heat transfer coefficients (HTCs) of water jacket cooling in [20], end winding spray oil cooling in [21], and the empirical rules (16) for airgap heat transfer in [22]. In (16)-(20), h_{air}, Nu, λ_{air}, Ta, Pr, Re, g, R_{ro}, v_{air}, α_{air}, and ω_{m} are the HTC between stator/rotor core and airgap, the Nusselt's number, the thermal conductivity of air, the Taylor's number, the Prandtl's number, the Reynold's number, the airgap length, the rotor outer radius, the kinematic viscosity of air, the thermal diffusivity of air, and the rotor angular speed, respectively. The ambient temperature is 20 °C. The objectives of the co-optimizations of EESMs for EV are listed in Table IV, including torque maximization and temperature minimization.

TABLE III
COOLING CONDITIONS OF EESMS FOR EV

Parameter	Value
Flow rate of frame water cooling/(L/min)	3.2
Water temperature, ϑ_{frc}/°C	20
HTC of frame water cooling/(W/(m^2·K))	3000
Flow rate of spray oil/(L/min)	3.0
Oil temperature, ϑ_{ewc}/°C	40
HTC of spray oil cooling/(W/(m^2·K))	600
HTC of airgap/(W/(m^2·K))	Empirical rule (16) [22]
Ambient temperature, ϑ_{a}/°C	20

TABLE IV
OPTIMIZATION OBJECTIVES OF EESMS FOR EV

Index	Target	Weight
Torque average value/(N·m)	> 210	9
ϑ_{max_all}/°C	< 170	1

$$h_{air} = \frac{Nu\lambda_{air}}{g} \tag{16}$$

$$Nu = \begin{cases} 2.2, Ta < 41 \\ 0.23Ta^{0.63}Pr^{0.27}, 41 < Ta < 100 \\ 0.42Ta^{0.5}Pr^{0.27}, Ta > 100 \end{cases} \tag{17}$$

$$Ta = Re\sqrt{\frac{g}{R_{ro}}} \tag{18}$$

$$Pr = \frac{\nu_{air}}{\alpha_{air}} \tag{19}$$

$$Re = \frac{R_{ro}\omega_m g}{\nu_{air}} \tag{20}$$

B. *Co-optimized EESMs*

ϑ_{max_all} and torque of all the individuals in the design optimizations of the EESMs are presented in Fig. 6. The pareto fronts are drawn, and the optimized designs are those on the knee points of the pareto fronts. The cross sections and parameter values of the optimized designs are presented in Fig. 7 and Table V. The EESM with stator-Cu/rotor-Cu windings has the highest torque (215.9 N·m) among all the optimized EESMs, while the EESM with stator-Al/rotor-Al windings has the lowest (162.7 N·m). The torque of the EESM with stator-Cu/rotor-Al windings (189.7 N·m) is higher than those of the other two EESMs with Al windings. ϑ_{max_all} of the EESM with only Al windings is close to 180 °C.

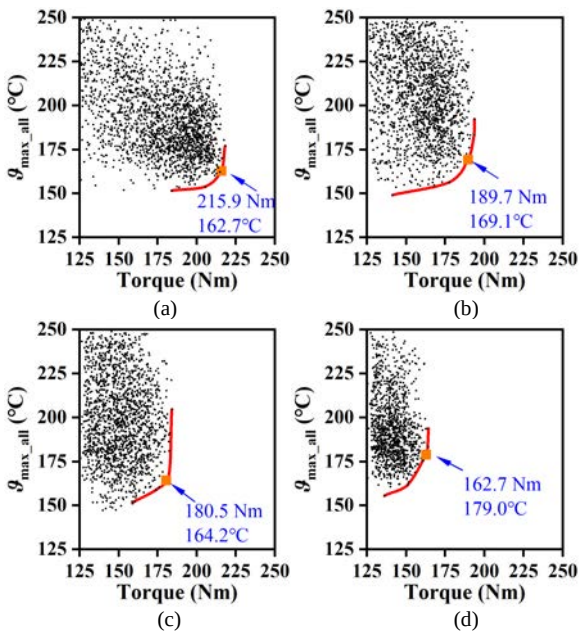

Fig. 6. ϑ_{max_all} and torque of all EESM individuals in co-optimizations. (a) Stator-Cu/rotor-Cu. (b) Stator-Cu/rotor-Al. (c) Stator-Al/rotor-Cu. (d) Stator-Al/rotor-Al.

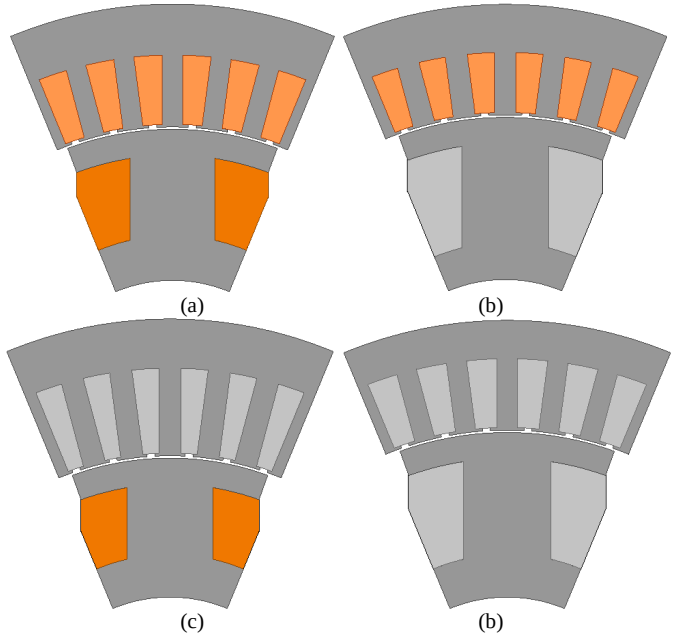

Fig. 7. Cross sections of all co-optimized EESM designs. (a) Stator-Cu/rotor-Cu. (b) Stator-Cu/rotor-Al. (c) Stator-Al/rotor-Cu. (d) Stator-Al/rotor-Al.

TABLE V
PARAMETER VALUES OF CO-OPTIMIZED EESMS

Parameter	Stator-Cu/ rotor-Cu	Stator-Cu/ rotor-Al	Stator-Al/ rotor-Cu	Stator-Al/ rotor-Al
t_{sy}/mm	15.8	15.0	15.2	11.9
w_t/mm	6.28	6.93	6.90	6.24
β_l/(°)	25.3	9.9	9.5	20.2
γ	2.253	2.275	2.707	2.043
σ	0.7112	0.7388	0.6806	0.7424
α_{ps}	0.91	0.89	0.88	0.88
w_p/mm	26.5	26.8	26.4	26.1
t_{ry}/mm	13.9	11.5	13.2	13.3
P_{Re_s}/W	5855.8	5873.1	6174.3	5676.9
P_{Re_r}/W	2599.2	2581.9	2280.7	2778.1
R_a/mΩ	110.9	140.0	162.4	173.0
R_f/mΩ	30.5	39.2	38.9	42.9
I_a/A	132.6	118.3	112.5	104.6
I_f/A	292.1	256.6	242.1	254.4
P_{iron_s}/W	340.5	317.9	342.4	278.9
P_{iron_r}/W	74.4	59.3	49.4	49.1
Torque/(N·m)	215.9	189.7	180.5	162.7

Steady-state three-dimensional (3-D) thermal FEA is conducted on all the co-optimized EESMs to validate the temperature calculated by the co-optimization method at the cooling conditions in Table III and with the losses in Table V as heat sources. The temperature distributions are shown in Fig. 8. The maximum and average winding temperatures calculated by thermal FEA and the co-optimization method are compared in Table VI. The difference in temperature is less than 2.5 °C, indicating that the temperatures calculated by the co-optimization method are accurate.

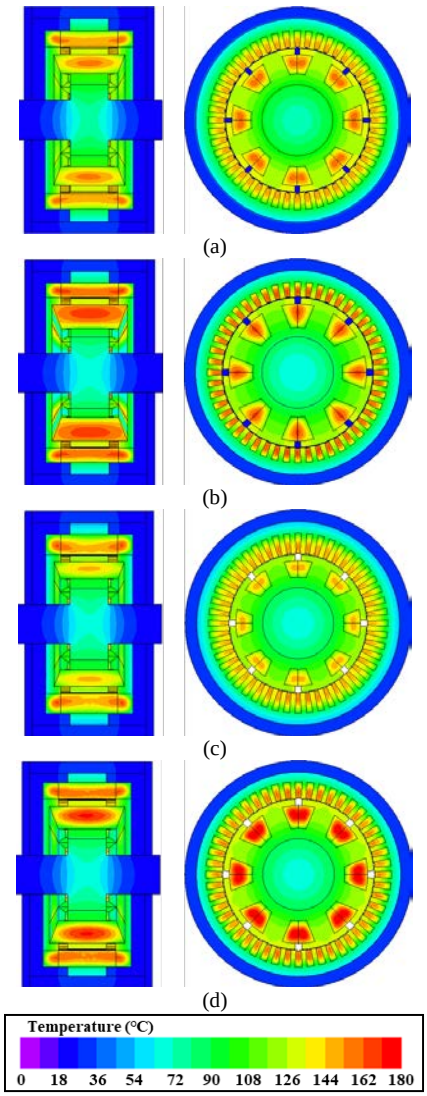

Fig. 8. Axial and radial temperature distributions of all EESMs at designed load operations calculated by thermal FEA. (a) Stator-Cu/rotor-Cu. (b) Stator-Cu/rotor-Al. (c) Stator-Al/rotor-Cu. (d) Stator-Al/rotor-Al.

TABLE VI
MAXIMUM AND AVERAGE WINDING TEMPERATURES (UNIT: °C) OF ALL EESMS CALCULATED BY CO-OPTIMIZATION METHOD AND THERMAL FEA

EESM	Temperature	LPTN	Thermal FEA	Error
Stator-Cu/rotor-Cu	$\vartheta_{max\_saw}/\vartheta_{saw}$	161.2/134.4	160.1/136.1	1.1/−1.7
	$\vartheta_{max\_sew}/\vartheta_{sew}$	162.7/141.5	163.0/142.3	−0.3/−0.8
	$\vartheta_{max\_raw}/\vartheta_{raw}$	162.5/140.4	162.1/142.3	0.4/−1.9
	$\vartheta_{max\_rew}/\vartheta_{rew}$	162.0/132.4	163.8/133.8	−1.8/−1.4
Stator-Cu/rotor-Al	$\vartheta_{max\_saw}/\vartheta_{saw}$	167.0/147.1	166.2/145.7	0.8/1.4
	$\vartheta_{max\_sew}/\vartheta_{sew}$	169.1/131.5	169.5/132.0	−0.4/−0.5
	$\vartheta_{max\_raw}/\vartheta_{raw}$	167.1/138.6	168.3/138.1	−1.2/0.5
	$\vartheta_{max\_rew}/\vartheta_{rew}$	166.4/124.7	166.7/122.9	−0.3/1.8
Stator-Al/rotor-Cu	$\vartheta_{max\_saw}/\vartheta_{saw}$	160.3/134.7	160.7/132.8	−0.4/1.9
	$\vartheta_{max\_sew}/\vartheta_{sew}$	164.2/123.1	166.6/122.7	−2.2/0.4
	$\vartheta_{max\_raw}/\vartheta_{raw}$	149.7/130.1	149.6/131.8	0.1/−1.7
	$\vartheta_{max\_rew}/\vartheta_{rew}$	152.4/122.8	151.5/123.4	0.9/−0.6
Stator-Al/rotor-Al	$\vartheta_{max\_saw}/\vartheta_{saw}$	161.6/140.1	163.3/139.3	−1.7/0.8
	$\vartheta_{max\_sew}/\vartheta_{sew}$	165.8/130.1	166.3/129.0	−0.5/1.1
	$\vartheta_{max\_raw}/\vartheta_{raw}$	179.0/149.6	180.8/147.4	−1.8/2.2
	$\vartheta_{max\_rew}/\vartheta_{rew}$	177.8/133.6	178.8/134.2	−1.0/−0.6

IV. COMPARISON OF ALL EESMS

In this section, the electromagnetic performance, driving cycle efficiency, material weight, and cost efficiency of all EESMs are compared.

A. *Electromagnetic Performance*

Electromagnetic FEA are conducted on all the co-optimized EESMs. The open-circuit airgap flux density, open-circuit flux linkage, open-circuit back electromagnetic force (EMF) at 3750 r/min, cogging torque, and load torque of all EESMs are compared in Fig. 9. In Fig. 9, A, B, C, and D represent the

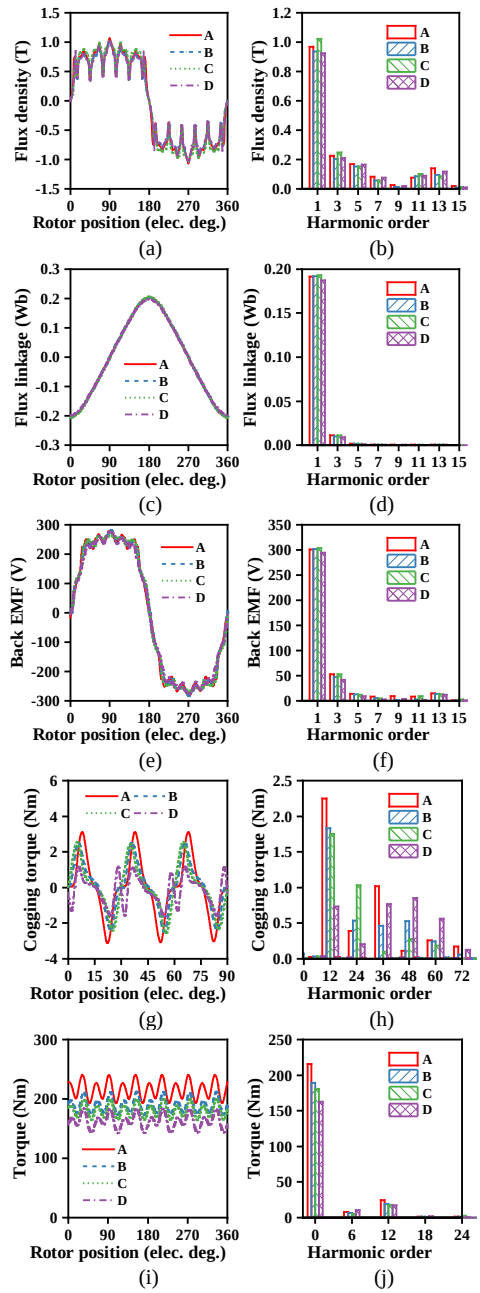

Fig. 9. Electromagnetic FEA results of all EESMs. (a) Open-circuit airgap flux density waveforms. (b) Open-circuit airgap flux density spectra. (c) Open-circuit flux linkage waveforms. (d) Open-circuit flux linkage spectra. (e) Open-circuit back EMF waveforms at 3750 r/min. (f) Open-circuit back EMF spectra at 3750 r/min. (g) Cogging torque waveforms. (h) Cogging torque spectra. (i) Load torque waveforms. (j) Load torque spectra.

co-optimized stator-Cu/rotor-Cu, stator-Cu/rotor-Al, stator-Al/ rotor-Cu, and stator-Al/rotor-Al EESMs, respectively. The magnetic field distributions of all the co-optimized EESMs at open-circuit and load operations are presented in Fig. 10.

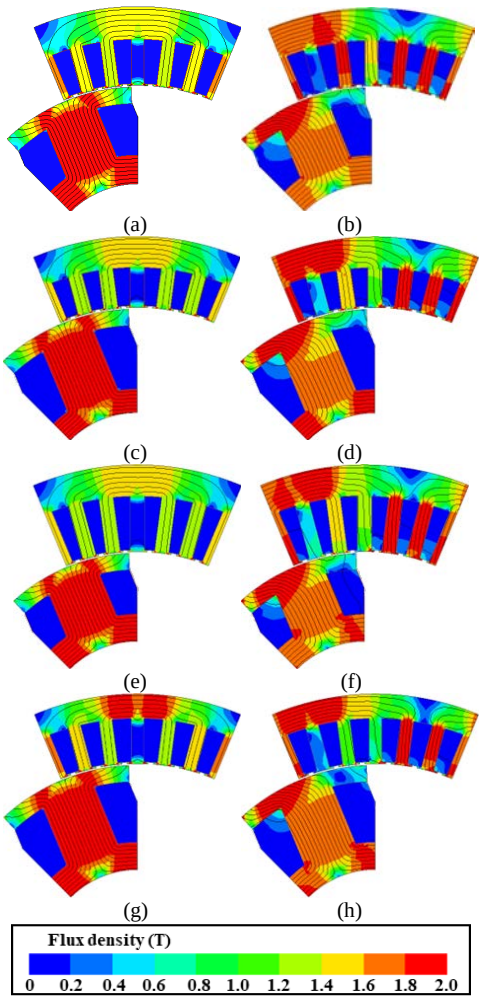

Fig. 10. Magnetic field distribution of all EESMs. (a) Stator-Cu/rotor-Cu, open-circuit. (b) Stator-Cu/rotor-Cu, load. (c) Stator-Cu/rotor-Al, open-circuit. (d) Stator-Cu/rotor-Al, load. (e) Stator-Al/rotor-Cu, open-circuit. (f) Stator-Al/rotor-Cu, load. (g) Stator-Al/rotor-Al, open-circuit. (h) Stator-Al/rotor-Al, load.

The relationship in no-load flux density among all the co-optimized EESMs is C > A > B > D. Although C has the lowest I_f according to Table V, the level of I_f is already very high for all EESMs and results in iron core magnetic saturation as shown in Fig. 10. Meanwhile, C has obviously lower split ratio and thus airgap radius than other EESMs, which leads to the highest airgap flux density [23]. Although C still has the highest open-circuit flux linkage and back EMF, the differences in flux linkage and back EMF among all the co-optimized EESMs are less obvious than that in airgap flux density because A, B, and D have higher split ratio and thus the airgap radius. The cogging torques of all the co-optimized EESMs are low due to high pole arc ratio and thus very uniform airgap. The significant differences in I_a, listed in Table V, of all the co-optimized EESMs result in significant differences in load torque (A > B > C > D) although the flux linkages are similar.

In Fig. 10, it can be observed that the iron core saturation level of the EESM with only Al windings is obviously higher than those of the other three EESMs due to thinner stator yoke, which indicates that the EESM with only Al windings has the highest magnetic reluctance, lowest flux linkage, and lowest back EMF fundamental magnitudes among all EESMs. The reason is that the conductivity of Al windings is low, and thus, both the stator and rotor slot areas of stator-Al/rotor-Al EESM should be as large as possible to reduce winding resistances for higher currents, which leads to a thin iron core. As presented in Table V, the stator-Al/rotor-Al EESM has less t_{sy}, w_t, and w_p than other EESMs.

B. Operational Performance for EV Application

To evaluate the operational performance of all EESMs in EV, the torque-speed and power-speed envelopes, efficiency maps, and new European driving cycle (NEDC) efficiencies are calculated. In this calculation, the DC bus voltage is 650 V, the maximum speed is 14,000 r/min [16], and the maximum I_a and I_f values of each EESM are those in Table V. The operational envelopes and NEDC profiles are presented in Fig. 11, where A, B, C, and D are the same as in Fig. 9. The vehicle profiles are given by Table VII [24]. The EESM with only Cu windings has the lowest base speed (3992 r/min), while the EESM with only Al windings has the highest base speed (4524 r/min) due to the lowest fundamental back EMF as already presented in Fig. 9(f). Although the EESM with only Al windings has the lowest torque, its maximum output power is compatible to that of the stator-Cu/rotor-Al EESM.

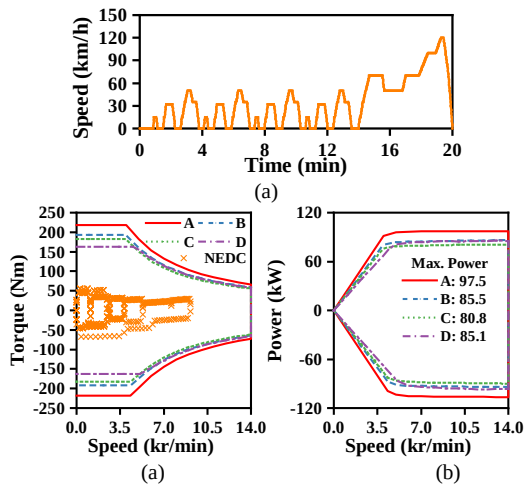

Fig. 11. Operational envelopes of all EESMs and NEDC profiles. (a) NEDC speed-time curve. (b) Torque-speed envelopes and NEDC operation points. (c) Power-speed envelopes.

TABLE VII
VEHICLE PARAMETERS FOR NEDC CALCULATION [24]

Parameter	Value	Parameter	Value
Curb weight/kg	1379	Drag coefficient	0.3
Wheel radius/m	0.3	Motor to wheel ratio	8.612
Front area/m^2	1.74	Transmission efficiency	95%
Rolling coefficient	0.0054		

The efficiency maps of all the co-optimized EESMs under the same conditions as in Fig. 11 are calculated and compared

in Fig. 12. The maximum efficiencies of the EESMs with stator-Cu/rotor-Cu, stator-Cu/rotor-Al, stator-Al/rotor-Cu, and stator-Al/rotor-Al windings are 95.1%, 94.4%, 94.0%, and 93.7%, respectively. The relationship in maximum efficiencies among all EESMs corresponds to that in output torque.

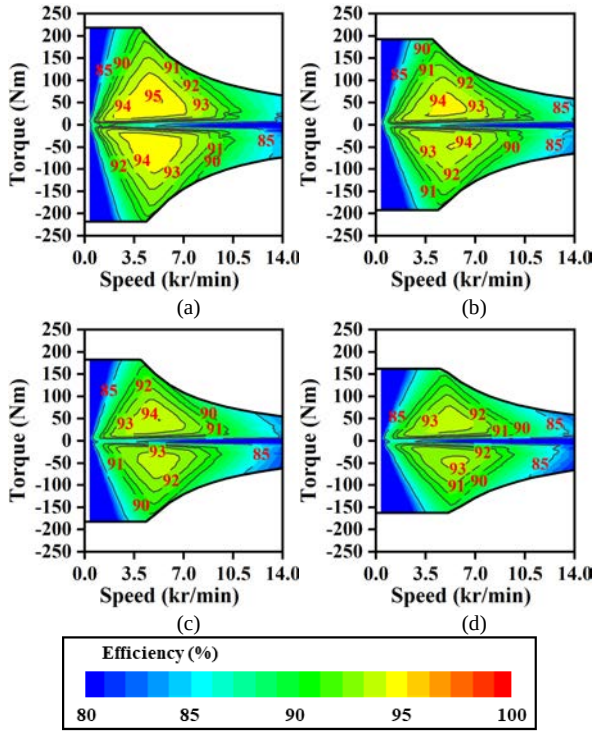

Fig. 12. Efficiency maps of all EESMs. (a) Stator-Cu/rotor-Cu. (b) Stator-Cu/rotor-Al. (c) Stator-Al/rotor-Cu. (d) Stator-Al/rotor-Al.

Based on the NEDC operational points and the efficiency maps, the NEDC efficiencies η_{NEDC} are calculated by (21). In (21), P_{Out_i}, P_{Loss_i}, and N are the output power of the i^{th} point, the loss of the i^{th} point, and the number of points in NEDC (N = 1200), respectively. The calculated NEDC efficiencies of all the co-optimized EESMs are compared in Table VIII.

$$\eta_{\mathrm{NEDC}} = \sum_{i=1}^{N} P_{\mathrm{Out}\_i} \Big/ \sum_{i=1}^{N} \left(P_{\mathrm{Out}\_i} + P_{\mathrm{Loss}\_i} \right) \times 100\% \tag{21}$$

TABLE VIII
NEDC EFFICIENCIES OF ALL EESMS

EESM	NEDC efficiency/%
Stator-Cu/rotor-Cu	87.52
Stator-Cu/rotor-Al	85.72
Stator-Al/rotor-Cu	84.56
Stator-Al/rotor-Al	83.39

Although the difference in maximum efficiency among all EESMs is less than 1.5%, there is an obvious difference in NEDC efficiency due to the obvious difference in the proportion of high efficiency region. The EESM with only Cu windings has 87.52% NEDC efficiency, while the EESM with only Al windings has 83.39% NEDC efficiency. The NEDC efficiency of the EESM with stator-Cu/rotor-Al windings is still 1.8% lower than that of the EESM with only Cu windings, but already higher than those of the other two EESMs with Al windings.

C. *Material Weight and Cost*

The material weight and cost of all the co-optimized EESMs are compared in Tables IX and X, respectively. The torque mass density and torque per cost are also listed in Tables IX and X, respectively. The prices per weight of laminations, Cu, and Al are 1.1, 8.5, and 2.6 \$/kg, respectively.

TABLE IX
WEIGHT (UNIT: KG) AND TORQUE DENSITY (UNIT: N·M/KG) OF ALL EESMS

EESM	Stator winding	Rotor winding	Stator core	Rotor core	Total	Torque density
Stator-Cu/rotor-Cu	4.39	5.63	7.37	5.41	22.80	9.47
Stator-Cu/rotor-Al	3.68	2.15	7.05	5.61	18.49	10.26
Stator-Al/rotor-Cu	1.42	4.09	8.03	4.90	18.44	9.79
Stator-Al/rotor-Al	1.45	2.06	6.81	6.12	16.44	9.90

TABLE X
COST (UNIT: \$) AND TORQUE PER COST (UNIT: N·M/\$) OF ALL EESMS

EESM	Stator winding	Rotor winding	Stator core	Rotor core	Total	Torque per cost
Stator-Cu/rotor-Cu	37.32	47.86	8.11	5.95	99.24	2.18
Stator-Cu/rotor-Al	31.28	5.59	7.76	6.17	50.80	3.73
Stator-Al/rotor-Cu	3.69	34.77	8.83	5.39	52.68	3.43
Stator-Al/rotor-Al	3.78	5.35	7.49	6.73	23.35	6.97

The weights of EESMs with stator-Cu/rotor-Al and stator-Al/rotor-Cu windings are around 19% less than that of the EESM with only Cu windings, and the EESM with only Al windings has 28% less weight. Since the torque reduction percentage of EESMs with Al windings to the EESM with only Cu windings is lower than the weight reduction percentage, the torque mass densities of all the EESMs with Al windings are higher than that of the EESM with only Cu winding. The EESM with stator-Cu/rotor-Al windings has the highest torque mass density (10.26 N·m/kg), 8.3% higher than that of the EESM with only Cu winding. Meanwhile, due to the lower mass density and lower price per weight of Al winding, the material costs of EESMs with stator-Cu/rotor-Al, stator-Al/rotor-Cu, and stator-Al/rotor-Al windings are only 53.1%, 51.2%, and 23.5% that of the EESM with only Cu windings. Correspondingly, the torque per cost of the EESMs with Al windings, which is the index of cost efficiency, are 71.1%, 57.3%, and 219.7% higher than that of the EESM with only Cu windings.

D. *Rotor Mechanical Stress*

The mechanical stresses on rotor core of all EESMs at the maximum speed 14,000 r/min are compared in Fig. 13 and Table XI, where the field windings are not shown. The elastic modulus and yield strength of laminations are 180 GPa and 420 MPa, respectively [25]. At 14,000 r/min, the rotor core mechanical stresses of all EESMs are within the yield strength. The rotor core of the EESM with stator-Al/rotor-Cu windings has the lowest stress due to the lowest split ratio and thus rotor outer radius. Compared to the EESM with only Cu windings, those with stator-Cu/rotor-Al and stator-Al/rotor-Al windings have around 10% higher stress at the pole shoe due to higher split ratio and rotor outer radius, but around 8% lower stress at the rotor yoke due to the lower rotor winding

weight as listed in Table XI. The mechanical stresses on rotor yokes are at least no less than those on rotor pole shoes. Therefore, the EESMs with rotor-Al windings have around 8% less maximum stresses on rotor core than that with only Cu windings.

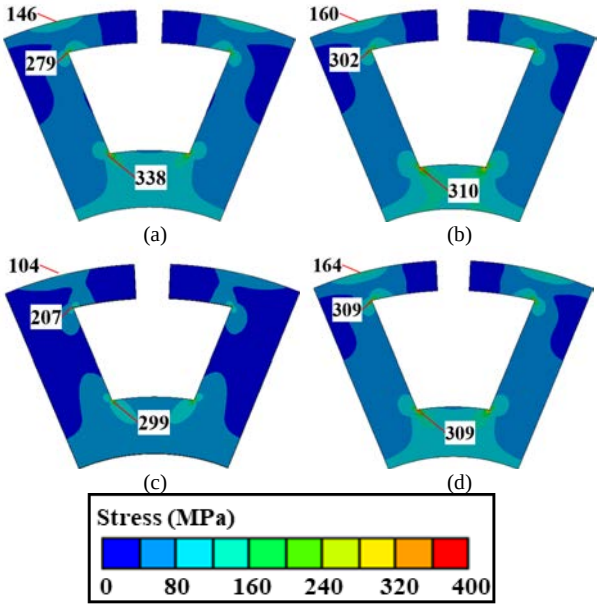

Fig. 13. Rotor core mechanical stresses at 14,000 r/min of all EESMs. (a) Stator-Cu/rotor-Cu. (b) Stator-Cu/rotor-Al. (c) Stator-Al/rotor-Cu. (d) Stator-Al/rotor-Al.

TABLE XI
ROTOR CORE MECHANICAL STRESS (UNIT: MPA) OF ALL EESMS

EESM	Rotor pole shoe	Rotor yoke
Stator-Cu/rotor-Cu	279	338
Stator-Cu/rotor-Al	302	310
Stator-Al/rotor-Cu	207	299
Stator-Al/rotor-Al	309	309

E. Discussion

Based on the above results, the EESMs with Al windings for both stator and/or rotor windings exhibit lower torque, lower output power, lower maximum efficiency, lower NEDC efficiency, lighter weight, lower cost, higher torque density, and higher torque per cost than the EESM with Cu windings for both stator and rotor windings, because the Al winding has higher resistivity but lower mass density and price per weight.

Among the EESMs with Al windings, the EESM with stator-Cu/rotor-Al windings has higher torque, torque density, and efficiency than the other two. Meanwhile, compared to the EESM with only Cu windings, the EESM with stator-Cu/rotor-Al windings already has 8.3% higher torque density and 71.1% higher torque per cost due to 12.1% less torque, 18.9% lighter material weight, and 48.8% lower material cost. Also, the EESMs with rotor-Al windings have 8% less rotor core maximum stress due to the reduced centrifugal force since the Al windings have lower mass density. Therefore, the EESM with stator-Cu/rotor-Al windings is a potential replacement of the EESM with only Cu windings considering its advantages in torque density and cost efficiency.

V. CONCLUSION AND FUTURE WORK

In this paper, the EESMs with Cu and/or Al windings in stator and/or rotor are designed using a simple electromagnetic-thermal co-optimization method and compared in terms of electromagnetic performance, operational performance, weight, and cost efficiency. Compared to the EESM with only Cu winding, the EESMs with Al windings exhibit lower torque capability, lower maximum output power, lower operational efficiency, lower driving cycle efficiency, but lighter material weight, lower material cost, higher torque mass density, and better cost efficiency. Also, due to the least torque reduction (12.1%), 8.3% higher torque density, 71.1% higher torque per cost, 61.8% lower rotor winding weight, and thus 8% lower maximum stress on the rotor core compared to the EESM with only Cu windings, the EESM with stator-Cu/rotor-Al windings can be a potential replacement of that with only Cu windings.

In the future, this comparative study will be validated by experiments by building and testing the scaled prototypes.

VI APPENDIX: COMPARISON UNDER IDENTICAL TORQUE STANDARD

The comparative study in this paper is conducted under the same outer radius, inner radius, stack length, resistive loss, DC bus voltage, and maximum speed. Although the differences in performance and cost efficiency can be confirmed, the torques of all the EESMs with different winding configurations are not identical. This is reasonable in research aspects, but the torque of all EESMs should be identical in the aspect of traction motor replacement in EVs. Therefore, a brief study is conducted by increasing the stack lengths of the EESMs with Al windings till their torques are the same as that of the EESM with only Cu windings while keeping their current profiles and bus voltage unchanged. In this way, the change in thermal performances of these EESMs can be ignored because the loss densities of windings and iron cores are unchanged. The increased stack lengths of the EESMs with Al windings are listed in Table XII according to the torque ratios between the EESM with only Cu windings and the EESMs with Al windings.

TABLE XII
STACK LENGTHS OF ALL EESMS FOR IDENTICAL TORQUE

EESM (identical torque, 215.9 N·m)	L_{stk}/mm
Stator-Cu/rotor-Cu	50.2 (unchanged)
Stator-Cu/rotor-Al	57.1
Stator-Al/rotor-Cu	60.0
Stator-Al/rotor-Al	66.6

By increasing the stack length, the weights and costs of active windings and iron cores, resistive losses of active windings, iron losses, and flux linkages increase linearly, while the weights and costs of end windings are unchanged. For the EV traction application, the operational envelopes, efficiency maps, and the NEDC efficiencies of the EESMs with identical torque are compared in Figs. 14, 15, and Table

XIII, respectively. The bus voltage, maximum speed, vehicle profiles, and NEDC operational points are the same as those in Section IV.B. In Fig. 14, B', C', and D' represent the stator-Cu/rotor-Al, stator-Al/rotor-Cu, and stator-Al/rotor-Al EESMs with increased stack lengths, respectively.

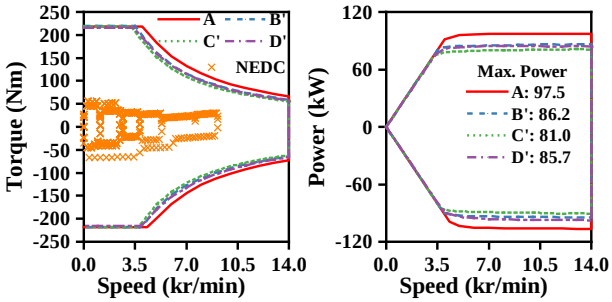

(a) (b)

Fig. 14. Operational envelopes of all EESMs with identical torque and NEDC profiles. (a) Torque-speed envelopes and NEDC operation points. (b) Power-speed envelopes.

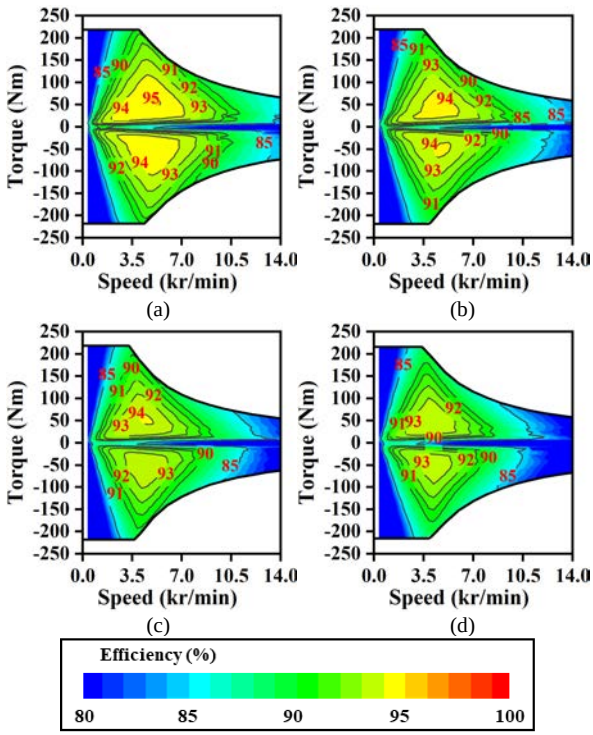

Fig. 15. Efficiency maps of all EESMs with identical torque. (a) Stator-Cu/rotor-Cu. (b) Stator-Cu/rotor-Al. (c) Stator-Al/rotor-Cu. (d) Stator-Al/rotor-Al.

TABLE XIII
NEDC EFFICIENCIES OF ALL EESMS WITH IDENTICAL TORQUE

EESM (identical torque)	NEDC efficiency/%
Stator-Cu/rotor-Cu	87.52
Stator-Cu/rotor-Al	86.44
Stator-Al/rotor-Cu	85.49
Stator-Al/rotor-Al	84.93

After increasing the stack lengths, the base speeds in the operational envelopes of the EESMs with Al windings are reduced under the same bus voltage, while the maximum output powers are almost the same as those before increasing the stack length (Fig. 11). The maximum efficiencies (B': 94.5%, C': 94.2%, D': 93.9%) of the EESMs with Al windings are also increased after increasing the stack lengths, while the NEDC efficiencies of B'/C'/D' are increased by 0.72%/0.93%/1.54%, respectively, because the end winding resistive losses are reduced due to the reduced currents at the same output torque.

The weight and cost of all the EESMs with identical torque are compared in Tables XIV and XV, respectively. After increasing the stack lengths of the EESMs with Al windings, their total material weights are still lighter than that of the EESM with only Cu windings, while the torque densities of the EESMs with Al windings are increased by 0.3–0.4 N·m/kg because the weights of end windings are unchanged. Correspondingly, the costs of the EESMs with Al windings and increased stack lengths are also increased, while their torques per cost are increased after the stack length increase because the costs of end windings are unchanged.

TABLE XIV
WEIGHT (UNIT: KG) AND TORQUE DENSITY (UNIT: N·M/KG) OF ALL EESMS WITH IDENTICAL TORQUE

EESM (identical torque)	Stator winding	Rotor winding	Stator core	Rotor core	Total	Torque density
Stator-Cu/rotor-Cu	4.39	5.63	7.37	5.41	22.80	9.47
Stator-Cu/rotor-Al	3.84	2.23	8.02	6.38	20.47	10.55
Stator-Al/rotor-Cu	1.51	4.32	9.60	5.86	21.29	10.14
Stator-Al/rotor-Al	1.60	2.25	9.03	8.12	21.00	10.28

TABLE XV
COST (UNIT: $) AND TORQUE PER COST (N·M/$) OF ALL EESMS WITH IDENTICAL TORQUE

EESM (identical torque)	Stator winding	Rotor winding	Stator core	Rotor core	Total	Torque per cost
Stator-Cu/rotor-Cu	37.32	47.86	8.11	5.95	99.24	2.18
Stator-Cu/rotor-Al	32.67	5.80	8.86	7.02	54.35	3.97
Stator-Al/rotor-Cu	3.92	36.74	10.55	6.44	57.65	3.74
Stator-Al/rotor-Al	4.16	5.84	9.94	8.93	28.87	7.48

However, as compared in Table XVI, the power densities of the EESMs with Al windings are decreased to lower than that of the EESM with only Cu windings after increasing the stack lengths, due to the similar output power under the same bus voltage and increased weight. Among all the EESMs with Al windings, only the one with stator-Cu/rotor-Al windings has a similar power density to that with only Cu windings under identical torque standard.

TABLE XVI
POWER DENSITIES (UNIT: KW/KG) OF ALL EESMS UNDER IDENTICAL-DIMENSION AND IDENTICAL-TORQUE STANDARDS

EESM	Identical dimensions (Sections III and IV)	Identical torque by increasing stack length
Stator-Cu/rotor-Cu	4.28	
Stator-Cu/rotor-Al	4.62	4.21
Stator-Al/rotor-Cu	4.38	3.80
Stator-Al/rotor-Al	5.18	4.08

According to the above analysis results under identical torque standard, the EESM with stator-Cu/rotor-Al windings still has the highest maximum efficiency, NEDC efficiency, and torque density among all the EESMs with Al windings, as

well as significantly improved cost efficiency and similar power density compared to the EESM with only Cu windings. Therefore, the stator-Cu/rotor-Al is still a good replacement of stator-Cu/rotor-Cu winding configuration of EESMs for EV traction under identical torque standards by stack length scaling.

REFERENCES

[1] C. Stancu, T. Ward, and K. M. Rahman *et al*., "Separately Excited Synchronous Motor with Rotary Transformer for Hybrid Vehicle Application," *IEEE Trans. on Ind. Appl.*, vol. 54, no. 1, pp. 223–232, Jan.-Feb. 2018.

[2] S. Estenlund, M. Alaküla, and A. Reinap, "PM-less Machine Topologies for EV Traction: a Literature Review," in *Proc. of 2016 Int. Conf. on Elect. Syst. for Aircr., Railway, Ship Propulsion and Road Veh. & Int. Transp. Electrific. Conf.*, Toulouse, France, Nov. 2016, pp. 1–6.

[3] H. Chen, J. F. Tang, and Y. J. Liu *et al*., "Electromagnetic Performance Investigation of a Brushless Electrically Excited Synchronous Machine for Long-distance Heavy-duty Electric Vehicles," *IEEE Trans. on Transp. Electrific.*, vol. 11, no. 1, pp. 225–235, Feb. 2025.

[4] F. Filippini, and N. Bianchi, "Design of an On-axis Electrically Excited Synchronous Motor for Heavy Commercial Vehicles," in *Proc. of 2024 IEEE Energy Convers. Congr. and Expo.*, Phoenix, AZ, USA, Oct. 2024, pp. 5185–5192.

[5] N. F. Jiao, Z. J. Li, and S. Mao *et al*., "Aircraft Brushless Wound-rotor Synchronous Starter-generator: a Technology Review," *IEEE Trans. on Power Electron.*, vol. 38, no. 6, pp. 7558–7574, Jun. 2023.

[6] Y. L. Wang, S. Nuzzo, and H. Zhang *et al*., "Challenges and Opportunities for Wound Field Synchronous Generators in Future More Electric Aircraft," *IEEE Trans. on Transp. Electrific.*, vol. 6, no. 4, pp. 1466–1477, Dec. 2020.

[7] T. Z. Xiao, Z. T. Ran, and Z. Q. Zhu *et al*., "Optimal Stator/rotor Copper Loss Ratio for Maximum Torque of Electrically Excited Machines," *IEEE Trans. on Ind. Appl.*, vol. 61, no. 1, pp. 137–150, Jan.-Feb. 2025.

[8] W. P. Chai, and B. Kwon, "Design of an Asymmetric Rotor Pole for Wound Field Synchronous Machines," *CES Trans. on Elect. Mach. and Syst.*, vol. 5, no. 4, pp. 321–327, Dec. 2021.

[9] G. Petrelli, G. Cutuli, and S. Nuzzo *et al*., "On Comparing Aluminum and Copper in Wound Field Synchronous Motors for Traction Applications," in *Proc. of 2024 Int. Conf. on Elect. Mach.*, Torino, Italy, Sept. 2024, pp. 1–7.

[10] A. Gneiting, F. Burkard, and N. Parspour, "Performance Evaluation of Aluminum and Copper Windings in Electrically Excited Synchronous Machines Considering Drive Cycle Efficiency and Maximum Continuous Power," in *Proc. of 2025 IEEE Int. Elect. Mach. & Drives Conf.*, Houston, TX, USA, May 2025, pp. 1117–1122.

[11] G. Cutuli, S. Nuzzo, and D. Barater *et al*., "Replacing Copper with Aluminum in Hairpin Windings Motors Intended for Utility Cars," *IEEE J. of Emerg. and Sel. Top. in Ind. Electron.*, vol. 6, no. 3, pp. 864–876, Jul. 2025.

[12] V. Madonna, C. M. Meano, and S. Mafrici *et al*., "Copper vs. Aluminium Winding SRMs: a Multidisciplinary Performance Assessment," in *Proc. of 12th International Conference on Power Electronics, Machines and Drives*, Brussels, Belgium, Oct. 2023, pp. 49–56.

[13] S. Mukundan, H. Dhulipati, and L. Chauvin *et al*., "Comparative Performance Analysis of Copper and Aluminum Wound Fractional-slot PMSMs for High-speed Traction Application," in *Proc. of 2019 22nd Int. Conf. on Elect. Mach. and Syst.*, Harbin, China, Aug. 2019, pp. 1–6.

[14] J. D. Widmer, R. Martin, and B. C. Mecrow, "Precompressed and Stranded Aluminum Motor Windings for Traction Motors," *IEEE Trans. on Ind. Appl.*, vol. 52, no. 3, pp. 2215–2223, May-Jun. 2016.

[15] P. Falletta, G. Cutuli, and S. G. Barbieri *et al*., "Comparison between Aluminum and Copper Hairpins on the Torsional-flexural Instability Phenomenon in the Bending Process," in *Proc. of 2025 IEEE Workshop on Elect. Mach. Des., Control and Diagnosis*, Valletta, Malta, Apr. 2025, pp. 1–6.

[16] T. A. Burress, S. L. Campbell, and C. L. Coomer *et al*., "Evaluation of the 2010 Toyota Prius Hybrid Synergy Drive System," Oak Ridge, TN, USA, Oak Ridge National Lab., Tech. Rep. ORNL/TM-2010/253, Mar. 2011.

[17] G. Bertotti, "General Properties of Power Losses in Soft Ferromagnetic Materials," *IEEE Trans. on Magn.*, vol. 24, no. 1, pp. 621–630, Jan. 1988.

[18] P. O. Gronwald, and T. A. Kern, "Traction Motor Cooling Systems: a Literature Review and Comparative Study," *IEEE Trans. on Transp. Electrific.*, vol. 7, no. 4, pp. 2892–2913, Dec. 2021.

[19] D. W. Liang, T. Z. Xiao, and Z. Q. Zhu *et al*., "Maximum Winding Temperature Predictions in Electrically Excited Synchronous Machines," *IEEE Trans. on Energy Convers.*, vol. 41, no. 1, pp. 484–502, Mar. 2026.

[20] Y. H. Gai, M. Kimiabeigi, and Y. C. Chong *et al*., "Cooling of Automotive Traction Motors: Schemes, Examples, and Computation Methods," *IEEE Trans. on Ind. Electron.*, vol. 66, no. 3, pp. 1681–1692, Mar. 2019.

[21] C. Liu, Z. Y. Xu, and D. Gerada *et al*., "Experimental Investigation on Oil Spray Cooling with Hairpin Windings," *IEEE Trans. on Ind. Electron.*, vol. 67, no. 9, pp. 7343–7353, Sept. 2020.

[22] D. W. Liang, Z. Q. Zhu, and J. H. Feng *et al*., "Influence of Critical Parameters in Lumped-parameter Thermal Models for Electrical Machines," in *Proc. of 2019 22nd Int. Conf. on Elect. Mach. and Syst.*, Harbin, China, Aug. 2019, pp. 1–6.

[23] Y. Li, Z. Q. Zhu, and D. W. Liang *et al*., "Comparative Study of PM Demagnetization in Air- and Iron-cored Halbach Machines," *IEEE Trans. on Ind. Appl.*, Early Access, pp. 1–13, Nov. 2025.

[24] J. Goss, M. Popescu, and D. Staton, "A Comparison of an Interior Permanent Magnet and Copper Rotor Induction Motor in a Hybrid Electric Vehicle Application," in *Proc. of 2013 Int. Electr. Mach. & Drives Conf.*, Chicago, IL, USA, May 2013, pp. 220–225.

[25] K. O. Kim, Y. H. Jung, and J. C. Park *et al*., "Comparative Study of Mechanical and Electrical Characteristics of High-strength and Conventional Electrical Steel for EV Traction High-speed Multilayer IPMSM Using Rare-earth Free PM," *IEEE Trans. on Magn.*, vol. 59, no. 11, pp. 1–5, Nov. 2023.

Tianzheng Xiao (Graduate Student Member, IEEE) was born in Jiangxi, China, in 1998. He received the B. Eng. and M. Sc. degrees in electrical engineering from Huazhong University of Science and Technology, Wuhan, China in 2019 and 2022, respectively. He is currently working toward the PhD degree since 2022 in electrical engineering at the University of Sheffield, Sheffield, UK.

His research interests include design and analysis of permanent magnet and electrically excited synchronous electrical machines, as well as the study of losses in electrical machines.

Zi Qiang Zhu (M'90, SM'00, F'09) received the B.Eng. and M.Sc. degrees from Zhejiang University, Hangzhou, China, in 1982 and 1984, respectively, and the Ph.D. degree from the University of Sheffield, Sheffield, UK, in 1991, all in electrical engineering.

From 1988 to 2025, he was with the University of Sheffield, as Professor (1997–2025), Royal Academy of Engineering/Siemens Research Chair (2014–2023), and Head of the Electrical Machines and Drives

Research Group (2008–2025). Since 2025, he has been a Chair Professor at the Hong Kong Polytechnic University, Hong Kong, China. He is Founding Director of four industrial research centers, including the Sheffield Siemens Gamesa Renewable Energy Research Centre and Midea Shanghai Electric Machines and Control Systems Research Centre. His current major research interests include design and control of permanent magnet machines and drives for applications ranging from electrified transportation through renewable energy to domestic appliance, robots, and automation. He is a Fellow of the Royal Academy of Engineering, UK, the Institute of Electrical and Electronics Engineers (IEEE), USA., the Institute of Engineering and Technology (IET), UK, and the Chinese Society for Electrical Engineering (CSEE) and China Electrotechnical Society (CES).

Ziad Azar received the B.Eng. degree in electrical engineering from the University of Damascus, Damascus, Syria, in 2003, and the M.Sc. degree in electronic and electrical engineering and the Ph.D. degree in electrical engineering from the University of Sheffield, Sheffield, UK, in 2008 and 2012, respectively.

From 2008 to 2012, Ziad was a Research Associate at the University of Sheffield, with major research interests covering modelling, design, and analysis of permanent magnet, as well as magnetless brushless machines for automotive applications. From 2012 to 2024, Ziad was with Siemens Gamesa Renewable Energy, and the last role was the Technology Development Manager with a focus on the development and validation of generator technologies and topologies to enhance the capability, efficiency, and reliability of direct-drive wind power turbines. Ziad is currently the Head of Portfolio Strategy Management at Siemens Energy Industrial Turbomachinery, with the responsibilities of the product development and ownership, product life-cycle management, and strategy development.